

---

---

# Preclinical Evaluation of $^{68}\text{Ga}$ -Labeled 1,4,7-Triazacyclononane-1,4,7-Triacetic Acid-Ubiquicidin as a Radioligand for PET Infection Imaging

Thomas Ebenhan<sup>1-3</sup>, Jan Rijn Zeevaart<sup>4</sup>, Jacobus D. Venter<sup>5</sup>, Thavendran Govender<sup>6</sup>, Gert H. Kruger<sup>2</sup>, Neil V. Jarvis<sup>3</sup>, and Mike M. Sathekge<sup>1</sup>

<sup>1</sup>Department of Nuclear Medicine, University of Pretoria and Steve Biko Academic Hospital, Pretoria, South Africa; <sup>2</sup>School of Chemistry, University of KwaZulu Natal, Durban, South Africa; <sup>3</sup>Research and Development, The South African Nuclear Energy Corporation, Pelindaba, Pretoria, South Africa; <sup>4</sup>Department of Science and Technology, Preclinical Drug Development Platform, North West University, Potchefstroom, South Africa; <sup>5</sup>Medical Research Council of South Africa, Pretoria, South Africa; and <sup>6</sup>Unit Catalysis, University of KwaZulu Natal, Durban, South Africa

Antimicrobial peptides such as ubiquicidin (UBI) are believed to differentiate between mammalian and bacterial or fungal cells.  $^{99\text{m}}\text{Tc}$ -UBI29-41 was previously tested for detecting infection in humans using SPECT. For the present study, the UBI fragment UBI29-41 (TGRAKRRMQYNRR) was conjugated to 1,4,7-triazacyclononane-triacetic acid (NOTA), radiolabeled with  $^{68}\text{Ga}$ , and investigated in a rabbit infection model. **Methods:**  $^{68}\text{Ga}$  was obtained from a 1.85-GBq  $^{68}\text{Ge}/^{68}\text{Ga}$  generator. New Zealand White rabbits were anesthetized with ketamine/medetomidine before tracer administration and placed in a clinical PET/CT scanner.  $^{68}\text{Ga}$ -1,4,7-triazacyclononane-1,4,7-triacetic-acid-ubiquicidin29-41 ( $^{68}\text{Ga}$ -NOTA-UBI29-41) was formulated in saline solution, and  $101 \pm 41$  MBq were administered intravenously. The tracer distribution was studied by PET/CT imaging in animals (a) that were healthy, (b) bearing muscular *Staphylococcus aureus* infections and turpentine oil-induced muscular inflammations, and (c) bearing ovalbumin-induced lung inflammations. Static PET/CT imaging was performed at different time intervals up to 120 min after injection. For calculation of target-to-nontarget ratios, standardized uptake values were normalized against healthy thigh muscle, representing nontargeted tissue. **Results:** PET/CT images of healthy animals showed predominant distribution in the kidneys, liver, and bladder; heart and spleen showed moderate, declining uptake, only. The biologic half-life in blood was 29 min. Urinary accumulation of  $^{68}\text{Ga}$ -NOTA-UBI29-41 peaked at  $3.8 \pm 0.91$  percentage injected dose per gram (%ID) at 120 min, and  $88 \pm 5.2$  %ID was recovered in total urine.  $^{68}\text{Ga}$ -NOTA-UBI29-41 imaging in (b) selectively visualized the muscular infection site and was differentiated from sterile inflammatory processes. Standardized uptake value ratios for muscles (infected/infamed) were  $2.9 \pm 0.93$ ,  $2.9 \pm 0.50$ ,  $3.5 \pm 0.86$ , and  $3.8 \pm 0.90$  at 5, 30, 60, and 90 min after injection, respectively. Rabbit lungs with asthma showed insignificant uptake. **Conclusion:**  $^{68}\text{Ga}$ -NOTA-UBI29-41 was strongly localized in bacteria-infected areas and minimally detected in a sterile inflammation area in rabbit muscles. The findings propose this compound to be an excellent

first-line PET/CT tracer to allow the distinguishing of infection from inflammation.

**Key Words:**  $^{68}\text{Ga}$  labeling; ubiquicidin; infection; UBI29-41; PET/CT Imaging

**J Nucl Med 2014; 55:308–314**

DOI: 10.2967/jnumed.113.128397

**I**nfectious diseases have a major impact on global morbidity and mortality despite advances in both diagnosis and treatment (1). The early identification and correct diagnosis of an active infection is crucial to its effective control or adequate treatment. Million of antibiotic doses are consumed unnecessarily, resulting in bacterial multidrug resistance and cost increases for therapy. Innovative diagnostic radiopharmaceuticals for detecting infection are of paramount importance because nuclear medicine techniques for detecting infections have the advantage of noninvasive whole-body imaging, which might be of great value in cases of occult infection. However, there are limitations, mainly the problem of differentiating between infectious and sterile inflammatory processes (2). To determine the correct course of treatment, clinicians need to be able to discriminate between sites of sterile inflammation and those that are infected by pathogenic microorganisms. Sites that are infected appear, at least superficially, similar to sites that are inflamed due to other reasons, such as trauma, ischemia, or the presence of foreign bodies such as implants or neoplasm (3). Radiolabeled leukocytes and  $^{67}\text{Ga}$ -citrate were the most commonly administered tracers for infection imaging (4), but because efficient current good manufacturing practices  $^{68}\text{Ge}/^{68}\text{Ga}$  generators became commercially available,  $^{68}\text{Ga}$ -citrate (5,6) and other novel  $^{68}\text{Ga}$ -labeled compounds such as  $^{68}\text{Ga}$ -siderophores (7) and  $^{68}\text{Ga}$ -apo-transferrin (8) were introduced for specific diagnosis of infected tissues.  $^{68}\text{Ga}$ -labeled peptides have also become relevant for diagnostic imaging because of their favorable pharmacokinetics (9). Interestingly, peptides with antimicrobial properties are found in abundance in mammals, amphibians, and plants, as a part of innate immunity against infection (10). Due to differences in electrostatic charges on the cell membrane or cell wall, human cationic antimicrobial peptides such as ubiquicidin (UBI) (11) are believed to differentiate between mammalian and bacterial or fungal

Received Jun. 28, 2013; revision accepted Oct. 22, 2013.

For correspondence or reprints contact: Mike Sathekge, Department of Nuclear Medicine, University of Pretoria and Steve Biko Academic Hospital, Private Bag X169, Pretoria, 0001, South Africa.

E-mail: mike.sathekge@up.ac.za

Published online Jan. 16, 2014.

COPYRIGHT © 2014 by the Society of Nuclear Medicine and Molecular Imaging, Inc.

cells (12). Fragments of UBI, namely UBI18-35 and UBI29-41 (TGRAKRRMQYNRR), were studied for their visualization of bacterial infections and sterile inflammatory processes (13).  $^{68}\text{Ga}$  can be labeled via a chelator-conjugated targeting molecule. One of these chelators is 1,4,7-triazacyclononane-triacetic acid (NOTA), which has a high affinity for  $^{68}\text{Ga}$  and therefore conjugates with peptides to functionalize these toward radiolabeling for prospective PET imaging (14). Preclinical publications (13,15,16) reported scintigraphic detection of bacterial and fungal infections using  $^{99\text{m}}\text{Tc}$ -UBI29-41. Clinical studies were performed by Melendez-Alafort et al. in 2004 and Akhtar et al. in 2005 administering  $^{99\text{m}}\text{Tc}$ -UBI29-41 for detecting infection using SPECT imaging (17,18). Key to this approach is that this peptide accumulates at infection sites but not in sterile inflammatory lesions. Studies in humans performed recently have applied  $^{99\text{m}}\text{Tc}$ -UBI29-41 to detect infection associated with fever of unknown origin (19) or used it for antibiotic therapy monitoring (20). For the present study, the UBI fragment UBI29-41 was conjugated with NOTA, subsequently radiolabeled with  $^{68}\text{Ga}$  and investigated in a preclinical rabbit infection model. The functional radiolabeling with  $^{68}\text{Ga}$  will allow image acquisition with PET/CT.

## MATERIALS AND METHODS

### General

All animal experiments were conducted according to the South African code of practice for the care and use of animals, after approval from the Medical Research Council ethics committee. Health surveillance was performed weekly for the duration of the experiments. Rabbits were randomly assigned to 1 of 3 groups (NZR-1, healthy condition [ $n = 8$ ]; NZR-2, muscular infection/inflammation [ $n = 7$ ]; NZR-3, pulmonary inflammation [asthma] [ $n = 3$ ]). Animals underwent 14-d antibiotics before the study to preclude random infections. Pharmaceutical grade chemicals were purchased from Merck. NOTA-UBI29-41 was obtained from GL Biochem. C18-SepPak cartridges were obtained from Waters Corp. Instant thin-layer chromatography silica gel (ITLC-SG) was purchased from PALL Life Science. Sterile Millex GV filters were obtained from Millipore. High-performance liquid chromatography-grade water was produced in-house using a Simplicity 185 Millipore system.

### Imaging of *Staphylococcus Aureus* Infection and Turpentine Inflammation in Muscles and Asthma in Lungs of Rabbits

*Staphylococcus aureus* 25923 was purchased from American Type Culture Collection. Bacilli stock was incubated overnight in nutrient broth at 37°C and agitation at 110 rpm. Sterile frozen aliquots ( $2 \times 10^8$  colony-forming units/cm<sup>3</sup>) were kept at -70°C. Saline solution (1 cm<sup>3</sup>) containing  $2 \times 10^8$  colony-forming units was injected into the right thigh muscle, and turpentine oil (1 cm<sup>3</sup>) was injected into the left hind thigh muscle of 7 rabbits (group NZR-2). PET/CT imaging was commenced 72 h after induction. Three rabbits (group NZR-3) were actively sensitized weekly for 4 wk with intraperitoneal injections of 1 cm<sup>3</sup> of an ovalbumin-containing solution (2.5 mg of ovalbumin in 1 part physiologic saline and 1 part of Alum [Pierce]). These rabbits were challenged by aerosol inhalation of 5% ovalbumin solution 1 wk after the last sensitization injection and again 24 h before PET/CT imaging. Rabbits were euthanized with a lethal dose of sodium pentobarbitone after imaging. For postmortem bacteriologic testing, sections of infected or inflamed sites of thighs were homogenized for cultivation in nutrient broth at 37°C. Bacterial identification was confirmed by biochemical testing. For histopathologic examination, sections of the sterile inflammation site, the infection site, and particular lung sections were fixed in 10% phosphate-buffered saline/buffered formalin and paraffin-embedded. Sections of 0.5  $\mu\text{m}$  were stained with hematoxylin and eosin and examined by light microscopy.

### Radiolabeling of UBI-NOTA29-41

Radiolabeling of NOTA-UBI29-41 was based on a  $^{68}\text{Ga}$ -DOTA-TATE labeling procedure (21). Briefly,  $^{68}\text{Ga}$ (III)chloride was eluted from a  $\text{SnO}_2$ -based  $^{68}\text{Ge}/^{68}\text{Ga}$  generator purchased from iThemba LABS using 0.6N HCl. Up to 95% activity yield was harvested in 2 cm<sup>3</sup> eluate. The sodium acetate-buffered  $^{68}\text{Ga}$  (pH 3.5–4) was incubated in the presence of 50 nM NOTA-UBI29-41 at 90°C for 15 min. In preparation for preclinical use,  $^{68}\text{Ga}$ -NOTA-UBI29-41 was purified from free  $^{68}\text{Ge}$ -,  $^{68}\text{Ga}$ -, and  $^{68}\text{Ga}$ -colloids using a C18-SepPak cartridge. The radiolabeled product was filtered through a Millex GV 0.22- $\mu\text{m}$  sterile filter and formulated in sterile saline solution.

### PET/CT Imaging

Subcutaneous injection of ketamine (15 mg/kg)/medetomidine (0.5 mg/kg) was given to induce sedation. Anesthesia was maintained by propofol/thiopental infusion. Whole-body PET/CT imaging with the patient supine was performed after the intravenous administration of  $29 \pm 13$  MBq of  $^{68}\text{Ga}$ -NOTA-UBI29-41 per kilogram. Images were acquired in 3-dimensional mode and reconstructed with and without attenuation correction (CT-based) using ordered-subset expectation maximization to yield axial, sagittal, and coronal slices (CT parameters: 120 kV; 120 mAs; slice thickness, 5 mm; pitch, 0.8 mm; matrix size, 512  $\times$  512). A minimum of three  $^{68}\text{Ga}$ -NOTA-UBI29-41-treated animals were scanned to achieve statistically significant data. Semi-quantitative analysis was performed using Siemens eSoft analytic software; 3-dimensional volumes of interest were drawn manually over the liver, kidneys, lung, heart, brain, spleen, bladder, brain, front and hind leg muscles, and infected and inflamed target tissues. When the half-life-corrected activity concentration of the organ volume of interest divided by the animal body weight and the injected dose (ID) was considered, the final values were expressed as organ SUV (standardized uptake value), as target organ-to-muscle ratios, or as percentage ID (%ID).

### Distribution of $^{68}\text{Ga}$ -NOTA-UBI29-41 in Rabbit Blood and Urine

Samples were collected from healthy rabbits (group NZR-1). About 1 cm<sup>3</sup> of blood was collected in heparinized tubes after intravenous administration of the radiopharmaceutical at 0, 1, 3, 5, 8, 12, 15, 30, 45, 60, and 90 min after injection. Urine (available volume  $\leq 5.5$  cm<sup>3</sup>) was harvested from catheterized bladders and collected after intravenous administration of the radiopharmaceutical at 0, 5, 15, 30, 45, 60, 90, and 120 min after injection. Samples were weighed, and radioactivity was measured using a CRC 25 ionization chamber (Capintec Inc.) and corrected for radioactivity decay. After 120 min, the bladder was drained to calculate the total urine recovery. Information gained from the blood and urine samples was used to draw time-activity curves to determine the biologic half-life and the elimination rate of the radiopharmaceutical.

### Analysis of $^{68}\text{Ga}$ Activity in Urine

Urine samples collected at 30, 60, and 120 min were analyzed using ITLC-SG (mobile phase, 0.1 M citric acid, pH 5) to calculate the percentage of free  $^{68}\text{Ga}$  activity per injected dose.

### Serum Integrity of $^{68}\text{Ga}$ -NOTA-UBI29-41

The tracer serum integrity was tested up to 180 min as described by Welling et al. (22) and analyzed by ITLC-SG and expressed as percentage recurrence of free  $^{68}\text{Ga}$ .

### Statistical Analysis

If systematic errors were nonexistent, outliers were determined by the Grubbs Test. Analytic data were expressed as mean value  $\pm$  SD.

**TABLE 1**  
Organ and Tissue Biodistribution of <sup>68</sup>Ga-NOTA-UBI29-41 in Healthy Rabbits

Organ or tissue	Percentage of injected dose (min) after injection*		
	30	60	120
Heart	0.66 ± 0.17	0.63 ± 0.31	0.55 ± 0.06
Liver	5.71 ± 2.43	3.82 ± 0.92	2.24 ± 0.96
Spleen	1.08 ± 0.52	0.73 ± 0.31	0.75 ± 0.09
Bladder, urinary tract	25.10 ± 6.09	27.55 ± 6.50	33.09 ± 7.24
Kidney	2.86 ± 1.10	4.23 ± 1.65	3.17 ± 0.71
Hind leg muscle	0.12 ± 0.05	0.10 ± 0.03	0.11 ± 0.02
Front leg muscle	0.11 ± 0.04	0.10 ± 0.03	0.10 ± 0.02
Lung	0.42 ± 0.18	0.46 ± 0.16	0.41 ± 0.06
Brain	0.05 ± 0.02	0.05 ± 0.02	0.06 ± 0.02

\*Values represent mean ± SD of *n* > 3 animals.

The significance of 2 mean values was calculated by a Student *t* test (paired and unpaired comparison). The level of significance was set at a *P* value of less than 0.05.

## RESULTS

### Radiolabeling and Tracer Injection

The complete labeling procedure including quality control was achieved in 36 ± 8 min. The product was stable in solution for up to 4 h. The product radioactivity achieved was 337 ± 91 MBq (*n* = 15), sufficient to inject 2 animals within 120 min. The product was sterile, pure (99.2% ± 0.46%, *n* = 13), and free of <sup>68</sup>Ge. The tracer was successfully injected with an activity concentration over the 3 groups of 27 ± 11 MBq (*n* = 8), 29 ± 15 MBq (*n* = 7), and 29 ± 13 MBq (*n* = 3) per kilogram for NZR-1, NZR-2, and NZR-3, respectively.

### PET/CT Imaging of Healthy Rabbits and Organ Biodistribution

Static images were obtained 30, 60, and 120 min after tracer injection, and radioactivity in target organs and tissues was quantified as %ID (Table 1) and SUV (Table 2). In Figure 1A, a representative PET image, taken at 60 min, shows highest activity accumulation in the urinary bladder, liver, and kidneys, representing renal excretion. The spleen, heart, and lung showed low uptake

with subsequent declining organ activity concentration. Minimal uptake of activity was observed in the musculoskeletal tissue; hence, the quantifications from the frontal leg triceps muscle was used as reference (nontargeted) tissue to calculate the target-to-nontarget (T/NT) ratios (Table 3). There was also no significant difference in the %ID values of frontal leg triceps and hind leg muscle at 30, 60, and 120 min.

### <sup>68</sup>Ga-NOTA-UBI29-41 Concentration in Blood and Urine of Healthy Rabbits

Results of the fluid analysis of <sup>68</sup>Ga-NOTA-UBI29-41 shows that the peak blood activity concentration was obtained 1 min after injection (0.68 ± 0.07 %ID/g) (Fig. 2A, *r*<sup>2</sup> = 0.886). A fast release of blood-bound activity is indicated by an exponential decline over 60 min, with an elimination rate of 1.44 %ID/h and a biologic blood half-life of 29 min. Between 30 and 60 min, an 18% decline of <sup>68</sup>Ga-NOTA-UBI29-41 activity concentration was noted. At approximately 90 min, no measurable activity was found in the obtained blood samples. Urine samples showed accumulating activity levels of <sup>68</sup>Ga-NOTA-UBI29-41 following a linear incline peaking at 3.8 ± 0.91 %ID/g at 120 min, with an accumulation rate of 1.72 %ID/h (Fig. 2B, *r*<sup>2</sup> = 0.969). After 120 min, the total urine recovery amounted to 88 ± 5.2 %ID (*n* = 3).

**TABLE 2**  
Organ and Tissue Concentration of <sup>68</sup>Ga-NOTA-UBI29-41 in Healthy Rabbits

Organ or tissue	SUV (min) after injection*		
	30	60	120
Heart	0.80 ± 0.24	0.65 ± 0.16	0.53 ± 0.24
Liver	1.91 ± 1.17	1.84 ± 1.32	0.67 ± 0.27
Spleen	1.65 ± 0.86	1.62 ± 0.95	0.74 ± 0.29
Bladder, urinary tract	19.96 ± 8.47	14.16 ± 4.24	10.65 ± 4.90
Kidney	3.20 ± 0.88	3.39 ± 0.74	2.85 ± 0.63
Hind leg muscle	0.25 ± 0.08	0.20 ± 0.04	0.12 ± 0.02
Front leg muscle	0.24 ± 0.05	0.20 ± 0.05	0.10 ± 0.03
Lung	0.60 ± 0.22	0.53 ± 0.22	0.35 ± 0.10
Brain	0.24 ± 0.11	0.16 ± 0.07	0.13 ± 0.07

\*Values represent mean ± SD of *n* > 3 animals.

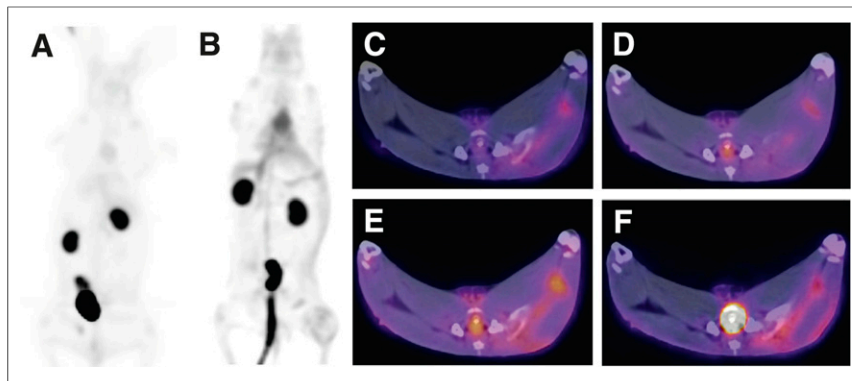


**FIGURE 1.** Coronal PET images acquired at 60 min after intravenous injection of 48–155 MBq of  $^{68}\text{Ga}$ -NOTA-UBI29-41 into healthy rabbits (NZR-1) (A) and 37–174 MBq of  $^{68}\text{Ga}$ -NOTA-UBI29-41 into rabbits with muscular infection (right thigh) and with sterile muscular inflammation muscle (left thigh) (NZR-2) (B). Axial PET/CT images displaying hind thighs 5 (C), 30 (D), 60 (E), and 90 (F) min after injection.

#### ITLC Analysis of $^{68}\text{Ga}$ Activity in Rabbit Urine

Urine samples were analyzed using ITLC at 30, 60, and 120 min. The peak activity for  $^{68}\text{Ga}^{3+}$  was detected with a retention factor of 0.05. Disintegration of the compound (free  $^{68}\text{Ga}$  activity percentage) was found for the 3 groups as  $0.88 \pm 0.35$ ,  $1.6 \pm 0.31$ , and  $4.2 \pm 0.55$  %ID, respectively.

#### Serum Integrity Analysis

$^{68}\text{Ga}$ -NOTA-UBI29-41 appeared stable in serum-challenged samples, with minimal recurrence of free  $^{68}\text{Ga}$  up to 120 min; the free  $^{68}\text{Ga}$  activity amounted to  $3.6 \pm 0.41$  %ID after 180-min incubation duration.

#### $^{68}\text{Ga}$ -NOTA-UBI29-41 Imaging of Infection

Noninvasive preclinical imaging was performed 72 h after induction to compare healthy animals (NZR-1) with bacteria-infected animals (NZR-2). The biodistribution of  $^{68}\text{Ga}$ -NOTA-UBI29-41 and its accumulation in both the muscular infection site and the inflammation site (Figs. 1A and 1B) was followed up to 90 min after injection of the radiopharmaceutical. The *Staphylococcus aureus*-bearing right thigh muscle was clearly visible in the PET/CT images, showing elevated uptake of  $^{68}\text{Ga}$ -NOTA-UBI29-41, compared with the contralateral thigh

muscle (bearing sterile inflammation), at 5, 30, 60, and 90 min after injection (Figs. 1C–1F), and the infection site showed gradual accumulation of the tracer over the time. The T/NT ratios representing muscular inflammation (Table 3) ranged from 0.98 to 1.25, with no significant difference, compared with normal muscular tissue ( $P > 0.349$ ). The maximum  $^{68}\text{Ga}$ -NOTA-UBI29-41 accumulation in an infected muscle was found 5.2 times higher than in normal muscle tissue at 60 min after injection. Additionally, the ratio of infected muscle to liver was moderate, with a maximum of 1.35 at 60 min.

#### $^{68}\text{Ga}$ -NOTA-UBI29-41 Uptake and Detection of Pulmonary Inflammation

The ability of  $^{68}\text{Ga}$ -NOTA-UBI29-41 to detect pulmonary inflammation was investigated by calculating tracer uptake and distribution in lungs. All acquired images were analyzed by calculating average whole-lung tissue SUV, which was related to the front triceps muscle SUV, yielding lung-to-muscle (L/M) ratios (Table 4). Images obtained at 30 and 60 min showed similar L/M ratios among the 3 groups. The (group-independent) L/M ratios followed a gradual, consistent incline ( $r^2 = 0.923$ ), amounting to  $1.95 \pm 0.44$  ( $n = 4$ ),  $2.46 \pm 0.53$  ( $n = 12$ ),  $2.51 \pm 0.48$  ( $n = 10$ ),  $2.73 \pm 1.01$  ( $n = 3$ ), and  $3.04 \pm 0.55$  ( $n = 3$ ) at 5, 30, 60, 90, and 120 min, respectively.

#### DISCUSSION

The present study was undertaken with NOTA-UBI29-41 to investigate it as a potential PET/CT imaging infection agent. Moreover, the molecule was tested for its feasibility to differentiate infection from pulmonary and extrapulmonary inflammation in rabbits.

Numerous studies were published evaluating  $^{99\text{m}}\text{Tc}$ -UBI29-41 in infected mice and rabbits (13,16,22,23) for SPECT only. One of the objectives has been to transfer the findings and therefore label the peptide fragment with the PET radionuclide  $^{68}\text{Ga}$  instead of  $^{99\text{m}}\text{Tc}$ , without compromising the infection-imaging

**TABLE 3**  
Accumulation of  $^{68}\text{Ga}$ -NOTA-UBI29-41 in *Staphylococcus Aureus*-Infected Rabbits

T/NT* ratio	PET/CT image acquisition (min) after injection†			
	5	30	60	90
Normal hind muscle to normal front muscle	1.02‡	0.99 ± 0.17	1.02 ± 0.19	ND
Infected muscle to normal muscle	3.16 ± 0.89	3.16 ± 0.75	4.35 ± 0.85	3.84 ± 1.53
Inflamed muscle to normal muscle	1.12 ± 0.14	1.12 ± 0.07	1.25 ± 0.25	0.98 ± 0.19
Infected muscle to inflamed muscle	2.86 ± 0.93	2.90 ± 0.50	3.54 ± 0.86	3.80 ± 0.90
Infected muscle to liver	0.97 ± 0.10	0.97 ± 0.52	1.35 ± 0.33	0.81 ± 0.59

\*Nontargeted tissue (frontal leg triceps).

†Values represent mean ± SD of > 3 animals/group.

‡Lung-to-muscle ratio calculated from single animal.

ND = value not determined.

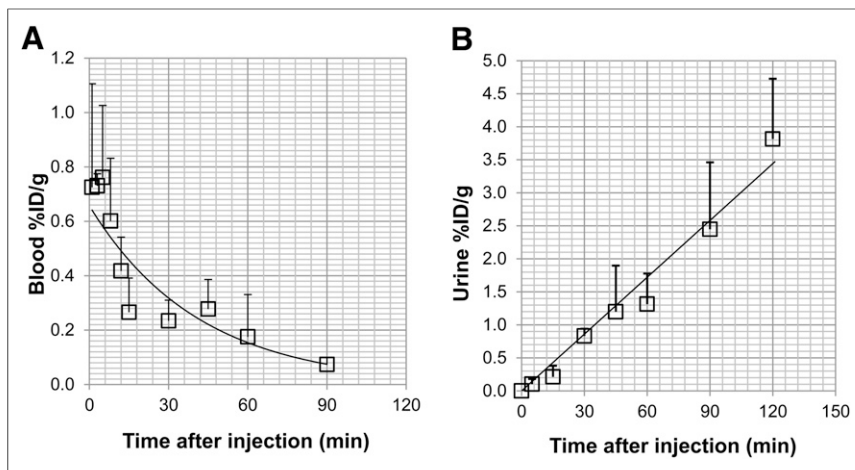


**FIGURE 2.** Activity concentration of  $^{68}\text{Ga}$ -NOTA-UBI29-41 in blood (A) and urine (B) obtained from healthy rabbits (group NZR-1). Animals were injected intravenously with  $96 \pm 35$  MBq/kg.

properties of UBI29-41. Whereas  $^{99\text{m}}\text{Tc}$  can be directly introduced to UBI29-41, because the Arg and Lys residues within the fragment support the complexation of  $^{99\text{m}}\text{Tc}$  (24), the complexation of  $^{68}\text{Ga}^{3+}$  to a peptide requires a chelating molecule. Such bifunctional chelators, of which DOTA is the most commonly used, are macrocyclic compounds designed as carriers for radiometals (25). We have selected NOTA as a chelator; with its 3 carboxyl and 3 tertiary amine residues it has been previously demonstrated to robustly complex  $^{68}\text{Ga}$  (26). Contrary to DOTA, the NOTA structure provides better selectivity for  $^{68}\text{Ga}^{3+}$ ; thus, it will form a conjugate, providing in vivo stability, and voids de-metalation and subsequent nonspecific accumulation of radiogallium.

NOTA-UBI29-41 was labeled using  $^{68}\text{Ga}$ , which was eluted from a tin dioxide-based generator, by fractionated elution, a simple but reliable step to reduce coelution of metal impurities such as Ge, Fe, or Zn (27). Labeling and purification was successfully performed for Ga-NOTA-UBI29-41, showing a labeling efficiency comparable to DOTA-conjugated peptides (21).

Healthy rabbits were scanned after  $^{68}\text{Ga}$ -NOTA-UBI29-41 administration to reveal generic tracer biodistribution and to obtain pharmacokinetic parameters in vivo. High uptake levels in the urinary bladder and kidneys dominated the  $^{68}\text{Ga}$ -NOTA-UBI29-41 biodistribution; however, it's acceptable for a PET agent, because

it can be easily kept under a hazardous radiation level and will seldom disturb image analysis. A  $^{99\text{m}}\text{Tc}$ -UBI29-41 study in healthy rabbits revealed gradual excretion for the kidneys, gradual decline in liver activity, and bladder accumulation up to 76 %ID at 120 min (28). Like Akhtar et al., our study confirmed the %ID accumulation in liver and bladder. Additionally, all organ or tissues (except kidneys) showed peak tracer concentration at 30 min, declining more or less gradually until 120 min. These findings indicate that NOTA conjugation to UBI29-41 may not interfere with its natural biodistribution. The present study also successfully determined the activity levels in blood and urine samples and subsequent calculation of a moderate biologic half-life of 29 min for  $^{68}\text{Ga}$ -NOTA-UBI29-41 in blood. Moreover, 88% of the injected activity dose

was recovered in total urine, 120 min after injection; a similar investigation was conducted in murine blood and urine by Welling et al. (22). The half-life of  $^{99\text{m}}\text{Tc}$ -labeled UBI29-41 ( $16\% \pm 0.85\%$ ) was compared with its scrambled UBI29-41 version ( $21\% \pm 1.2\%$ ), revealing a significant difference, when the amino acid sequence was compromised. The authors also reported the percentage distribution to blood plasma fraction and blood cells; most of the activity amount was associated with the plasma-to-platelet fraction (86 %ID) and less than 15 %ID within erythrocytes and leukocytes. We have positively tested the serum stability of  $^{68}\text{Ga}$ -NOTA-UBI29-41 up to 3 h. The urine analysis conducted by Welling et al. showed results similar to our findings, recovering 90 %ID activity in total urine. The 2 clinical studies performed with  $^{99\text{m}}\text{Tc}$ -UBI29-41 also support the hereby published findings of gradual blood-pool-activity decline and similar accumulation in urine (17,18). On the basis of our findings, we have reason to believe that uptake, distribution, and excretion of UBI29-41 were not significantly compromised by the conjugation with NOTA. It is noted, however, that alterations at the complexing moiety can cause a different metabolism of  $^{99\text{m}}\text{Tc}$ -UBI29-41 (i.e., the hydrazinonicotinamide-conjugation showed similar renal clearance and warranted the infection imaging in mice but the N(2)S(2)-conjugated  $^{99\text{m}}\text{Tc}$ -UBI29-41 showed hepatobiliary excretion and was subsequently

**TABLE 4**  
Pulmonary Distribution of  $^{68}\text{Ga}$ -NOTA-UBI29-41 in Rabbits: Quantification of Lung Tissue

T/NT* ratio (lung to muscle)	PET/CT image acquisition (min) after injection†				
	5	30	60	90	120
Healthy (NZR-1)	ND	$2.5 \pm 0.63$	$2.5 \pm 0.53$	ND	$3.0 \pm 0.55$
Infection/inflammation (NZR-2)	$1.9 \pm 0.53$	$2.5 \pm 0.79$	$2.2 \pm 0.49$	$2.7 \pm 1.01$	ND
Asthma (NZR-3)	$2.1^\ddagger$	$2.4 \pm 0.45$	$2.5 \pm 0.44$	ND	ND

\*Nontargeted tissue (frontal leg triceps).

†Values represent mean  $\pm$  SD of > 3 animals/group.

‡Lung-to-muscle ratio calculated from single animal.

ND = value not determined.

not recommended for detection of abdominal infection (29)). It is postulated that antimicrobial peptides bind selectively to bacterial cytoplasmic membranes, because the cationic peptide residues are capable of interacting electrostatically with those anionic regions of bacterial membranes (30,31). The rabbits of group NZR-2 were scanned at 5, 30, 60, and 90 min after injection to find the ideal, earliest and most selective time duration for the detection and differentiation of the muscular infection. We found higher  $^{68}\text{Ga}$ -NOTA-UBI29-41 uptake in infectious muscle than in normalized muscle in 7 of 7 rabbits and for all time durations up to 90 min, indicating sensitive binding by  $^{68}\text{Ga}$ -NOTA-UBI29-41. The muscular inflammation showed significantly lower accumulation for all time durations ( $P < 0.01$ ); 0 of 7 accumulations were significantly higher than in nontargeted muscle. T/NT ratios could differentiate between infection and inflammation from 20 min and increased gradually until 90 min after injection. Postmortem histopathologic analysis diagnosed a moderate, chronic, nonsuppurative myositis in the left thigh muscle. Distinct slides were also observed in the infected thigh; however, *Staphylococcus aureus* bacilli were exclusively detected in the right thigh muscle sample, confirming that the NOTA moiety did not compromise the ability of UBI29-41 to selectively visualize bacterial infection.

As the study scope is thought to be extended to noninvasive detection of airway infection, a required property of NOTA-UBI29-41 is an insensitivity to pulmonary inflammatory processes such as asthma. Rabbits sensitized with ovalbumin (NZR-3) will develop an early onset airway response that resembles human asthma with histopathologic changes, thus they can serve as a noninfectious model of inflammation (32). Airway and lung inflammations have been studied noninvasively, using mainly  $^{18}\text{F}$ -FDG in both animals and humans (33) and other imaging techniques such as functional MRI (fMRI) (34) and fluorescence-mediated tomography (FMT) (35). We found no significant increases in the L/M ratios in asthmatic inflamed lungs ( $P = 0.662$ ) and rabbit lungs of animals with an extrapulmonary infection and inflammation ( $P = 0.820$ ), compared with rabbit lungs in healthy condition. The postmortem histopathologic examination of the ovalbumin-challenged lungs positively confirmed a phenotype of asthmatic inflammation (diffuse moderate interstitial pneumonia was diagnosed with scattered heterophils, metaplasia, areas of emphysema, and areas of congestion). On the basis of this latter approach, we can preclude  $^{68}\text{Ga}$ -NOTA-UBI29-41 from accumulating in ovalbumin-challenged lungs and thereof it will not falsely detect an airway inflammation in rabbits.

## CONCLUSION

The results support that  $^{68}\text{Ga}$  NOTA-UBI29-41 is an efficient and sensitive tracer of in vivo imaging of infection.  $^{68}\text{Ga}$ -NOTA-UBI29-41 exhibited significant uptake ratios between muscular infection and inflammation. Further clinical evaluation of this novel metabolic tracer is warranted to investigate its potential use as a first-line PET/CT infection imaging agent.

## DISCLOSURE

The costs of publication of this article were defrayed in part by the payment of page charges. Therefore, and solely to indicate

this fact, this article is hereby marked "advertisement" in accordance with 18 USC section 1734. We gratefully acknowledge funding provided by the Nuclear Technologies in Medicine and the Biosciences Initiative (NTEMBI). No other potential conflict of interest relevant to this article was reported.

## ACKNOWLEDGMENTS

We thank Delene van Wyk, Cindy Davis, Roleen Celliers, and Brenda Mokaleng from Steve Biko Academic Hospital for assistance during PET/CT imaging and Dr. Daniel Goosen from Disease Control Africa for his veterinary expertise and for assistance on the animal monitoring.

## REFERENCES

1. Palestro CJ. Radionuclide imaging of infection: in search of the grail. *J Nucl Med*. 2009;50:671–673.
2. Sathekge M. The potential role of  $^{68}\text{Ga}$ -labeled peptides in PET imaging of infection. *Nucl Med Commun*. 2008;29:663–665.
3. Tossi A, Sandri L, Giangaspero A. Amphipathic, alpha-helical antimicrobial peptides. *Biopolymers*. 2000;55:4–30.
4. Knight LC. Non-oncologic applications of radiolabeled peptides in nuclear medicine. *Q J Nucl Med*. 2003;47:279–291.
5. Nanni C, Errani C, Boriani L, et al.  $^{68}\text{Ga}$ -citrate PET/CT for evaluating patients with infections of the bone: preliminary results. *J Nucl Med*. 2010;51:1932–1936.
6. Kumar V, Boddeti DK, Evans SG, Angelides S.  $^{68}\text{Ga}$ -citrate-PET for diagnostic imaging of infection in rats and for intra-abdominal infection in a patient. *Curr Radiopharm*. 2012;5:71–75.
7. Petrik M, Haas H, Dobrozemsky G, et al.  $^{68}\text{Ga}$ -siderophores for PET imaging of invasive pulmonary aspergillosis: proof of principle. *J Nucl Med*. 2010;51:639–645.
8. Kumar V, Boddeti DK, Evans SG, Roesch F, Howman-Giles R. Potential use of  $^{68}\text{Ga}$ -apo-transferrin as a PET imaging agent for detecting *Staphylococcus aureus* infection. *Nucl Med Biol*. 2011;38:393–398.
9. Ballinger JR, Solanki KK. What will be required to bring  $^{68}\text{Ga}$ -labelled peptides into routine clinical use? *Nucl Med Commun*. 2011;32:1109–1112.
10. Zasloff M. Antimicrobial peptides of multicellular organisms. *Nature*. 2002;415:389–395.
11. Hiemstra PS, van den Barselaar MT, Roest M, Nibbering PH, van Furth R. Ubiquicidin, a novel murine microbicidal protein present in the cytosolic fraction of macrophages. *J Leukoc Biol*. 1999;66:423–428.
12. Hancock RE, Patrzykat A. Clinical development of cationic antimicrobial peptides: from natural to novel antibiotics. *Curr Drug Targets Infect Disord*. 2002;2:79–83.
13. Welling MM, Paulusma-Annema A, Balter HS, Pauwels EK, Nibbering PH. Technetium-99m labelled antimicrobial peptides discriminate between bacterial infections and sterile inflammations. *Eur J Nucl Med*. 2000;27:292–301.
14. Guérin B, Ait-Mohand S, Tremblay MC, Dumulon-Perreault V, Fournier P, Benard F. Total solid-phase synthesis of NOTA-functionalized peptides for PET imaging. *Org Lett*. 2010;12:280–283.
15. Ferro-Flores G, Arteaga de Murphy C, Pedraza-Lopez M, et al. In vitro and in vivo assessment of  $^{99m}\text{Tc}$ -UBI specificity for bacteria. *Nucl Med Biol*. 2003;30:597–603.
16. Nibbering PH, Welling MM, Paulusma-Annema A, Brouwer CP, Lupetti A, Pauwels EK.  $^{99m}\text{Tc}$ -Labeled UBI 29-41 peptide for monitoring the efficacy of antibacterial agents in mice infected with *Staphylococcus aureus*. *J Nucl Med*. 2004;45:321–326.
17. Akhtar MS, Qaisar A, Irfanullah J, et al. Antimicrobial peptide  $^{99m}\text{Tc}$ -ubiquicidin 29-41 as human infection-imaging agent: clinical trial. *J Nucl Med*. 2005;46:567–573.
18. Meléndez-Alafort L, Rodríguez-Cortés J, Ferro-Flores G, et al. Biokinetics of  $^{99m}\text{Tc}$ -UBI 29-41 in humans. *Nucl Med Biol*. 2004;31:373–379.
19. Sepúlveda-Méndez J, de Murphy CA, Rojas-Bautista JC, Pedraza-Lopez M. Specificity of  $^{99m}\text{Tc}$ -UBI for detecting infection foci in patients with fever in study. *Nucl Med Commun*. 2010;31:889–895.
20. Nazari B, Azizmohammadi Z, Rajaei M, et al. Role of  $^{99m}\text{Tc}$ -ubiquicidin 29-41 scintigraphy to monitor antibiotic therapy in patients with orthopedic infection: a preliminary study. *Nucl Med Commun*. 2011;32:745–751.

21. Rossouw DD, Breeman WA. Scaled-up radiolabelling of DOTATATE with  $^{68}\text{Ga}$  eluted from a  $\text{SnO}_2$ -based  $^{68}\text{Ge}/^{68}\text{Ga}$  generator. *Appl Radiat Isot.* 2012;70:171–175.
22. Welling MM, Mongera S, Lupetti A, et al. Radiochemical and biological characteristics of  $^{99\text{m}}\text{Tc}$ -UBI 29-41 for imaging of bacterial infections. *Nucl Med Biol.* 2002;29:413–422.
23. Akhtar MS, Khan ME, Khan B, et al. An imaging analysis of  $^{99\text{m}}\text{Tc}$ -UBI (29-41) uptake in *S. aureus* infected thighs of rabbits on ciprofloxacin treatment. *Eur J Nucl Med Mol Imaging.* 2008;35:1056–1064.
24. Meléndez-Alafort L, Ramirez Fde M, Ferro-Flores G, Arteaga de Murphy C, Pedraza-Lopez M, Hnatowich DJ. Lys and Arg in UBI: a specific site for a stable Tc-99m complex? *Nucl Med Biol.* 2003;30:605–615.
25. De León-Rodríguez LM, Kovacs Z. The synthesis and chelation chemistry of DOTA-peptide conjugates. *Bioconj Chem.* 2008;19:391–402.
26. Moore DAF, Fanwick PE, Welch MJ. A novel hexachelating amino-thiol ligand and its complex with gallium(III). *Inorg Chem.* 1990;29:672–676.
27. de Blois E, Sze Chan H, Naidoo C, Prince D, Krenning EP, Breeman WA. Characteristics of  $\text{SnO}_2$ -based  $^{68}\text{Ge}/^{68}\text{Ga}$  generator and aspects of radiolabelling DOTA-peptides. *Appl Radiat Isot.* 2011;69:308–315.
28. Akhtar MS, Iqbal J, Khan MA, et al.  $^{99\text{m}}\text{Tc}$ -labeled antimicrobial peptide ubi-ucidin (29-41) accumulates less in *Escherichia coli* infection than in *Staphylococcus aureus* infection. *J Nucl Med.* 2004;45:849–856.
29. Welling MM, Visentin R, Feitsma HI, Lupetti A, Pauwels EK, Nibbering PH. Infection detection in mice using  $^{99\text{m}}\text{Tc}$ -labeled HYNIC and  $\text{N}_2\text{S}_2$  chelate conjugated to the antimicrobial peptide UBI 29-41. *Nucl Med Biol.* 2004;31:503–509.
30. Yeaman MR, Yount NY. Mechanisms of antimicrobial peptide action and resistance. *Pharmacol Rev.* 2003;55:27–55.
31. Lupetti A, Nibbering PH, Welling MM, Pauwels EK. Radiopharmaceuticals: new antimicrobial agents. *Trends Biotechnol.* 2003;21:70–73.
32. Bayat S, Strengell S, Porra L, et al. Methacholine and ovalbumin challenges assessed by forced oscillations and synchrotron lung imaging. *Am J Respir Crit Care Med.* 2009;180:296–303.
33. Chen DL, Schuster DP. Imaging pulmonary inflammation with positron emission tomography: a biomarker for drug development. *Mol Pharm.* 2006;3:488–495.
34. Tigani B, Cannet C, Karmouty-Quintana H, et al. Lung inflammation and vascular remodeling after repeated allergen challenge detected noninvasively by MRI. *Am J Physiol Lung Cell Mol Physiol.* 2007;292:L644–L653.
35. Korideck H, Peterson JD. Noninvasive quantitative tomography of the therapeutic response to dexamethasone in ovalbumin-induced murine asthma. *J Pharmacol Exp Ther.* 2009;329:882–889.